Microfluidic method for determining drop-drop coalescence and contact times in flow

Marcin Dudek [1], Diana Fernandes [2], Eirik Helno Herø [3] and Gisle Øye[1]*

[1] Ugelstad Laboratory, Department of Chemical Engineering, Norwegian University of Science and Technology (NTNU), Trondheim, Norway

[2] Department of Chemical Engineering, Polytechnic of Porto – School of Engineering (ISEP) Porto, Portugal

[3] Department of Chemical Engineering, Norwegian University of Science and Technology (NTNU), Trondheim, Norway

* Corresponding author: marcin.dudek@ntnu.no

ABSTRACT

Coalescence kinetics is an important parameter when describing the stability of dispersions. A number of methods to measure coalescence time are available, however they often take long time and do not allow working with small droplets or coalescence in flow. Here we present a new microfluidic method for recording and analysing hundreds or thousands of individual droplet interactions in flow. Our method allows to extract information about both the coalescence and the contact times of drops. In addition, we can distinguish the coalescence events by the droplet size, as well as the approach velocity of the colliding droplets. We validated the proposed methodology by systematically changing a number parameters of the experiment (salinity, oil composition, presence of surfactant,

temperature). The increase of salinity lead to compression of the double layer and decreased coalescence time. A difference was found when studying coalescence of heptane, xylene and dodecane, which was attributed to their hydrophobicity and viscosity. The addition of surfactant caused a significant increase of coalescence time through additional repulsion and Marangoni effect, while higher temperature caused faster coalescence of droplets. We also found that increased approach velocity generally reduced both contact and coalescence times, up to certain (critical) value. Beyond that, no coalescence was observed.

KEYWORDS: Emulsion, coalescence time, contact time, approach velocity, microfluidics, droplet

1. INTRODUCTION

The stability of emulsions is a key aspect of many industrial processes. On the one hand, cosmetics, pharmaceutical and food industries aim to produce stable emulsions, which in the end extends the shelf life of their products. On the other hand, processes involving separation of phases require destabilizing emulsions during the treatment or purification operations. This is the case for crude oil and natural gas production, where the breakage and separation of foams, water-in-oil or oil-in-water emulsions is crucial for process efficiency [1].

Emulsions are kinetically stabilized dispersions. A number of factors contribute to their stability: chemical composition and properties, presence of electrolyte, type and concentration of surfactants, droplet size distribution, temperature and more [2]. All these parameters affect the magnitude of the attractive and repulsive forces between droplets in an emulsion. The attraction is due to the short-range van der Waals forces, originating from

various dipole-dipole interactions. For hydrophobic interfaces in water, additional attractive forces (often called hydrophobic forces) can arise due to the presence of dissolved gas molecules or the molecular structuring of water near hydrophobic surfaces [3]. The repulsive forces originate from overlapping electrical double layers or steric interactions caused by the presence of non-ionic surfactants or polymers. In addition, the Marangoni effect may influence the stability of emulsions [2].

Coalescence is an important mechanism during destabilization of emulsions. It is commonly described with the film drainage model, which distinguishes three individual stages of the process: collision, film drainage and film rupture [4]. Collisions between drops can occur through agitation, gravity forces or Brownian motion. A thin film of the continuous phase is formed between two approaching droplets. In order for these drops to coalesce, the film has to be drained to a critical thickness, at which strong attractive forces disrupt the film and enable the two droplets to merge into one. The time necessary for the film to be drained (i.e. drainage time – t_{dr}) is controlling the kinetic aspects of the emulsion destabilization through coalescence. According to various models, summarized in a review paper by Liao and Lucas [5], it typically depends on the droplet size, dispersed and continuous fluid properties, interaction forces and other. Not every collision, however, leads to coalescence. After contact, the droplets can detach and flow apart. This ratio of collisions and coalescence events is often termed as the coalescence probability. In many models it is proportional to $\exp(-t_c/t_{dr})$, where the t_c is the contact time, which is also an important feature in emulsion destabilization and is defined as the average time that droplets stay in contact that results either in coalescence or detachment [4]. The contact time is affected by the hydrodynamic conditions and the net interaction forces, being the result of the attractive and repulsive interactions in the system. The former will be determined by the

approach velocity between the droplets, which is a major factor in the coalescence process [6, 7]. In general, the shorter the t_c, the smaller the chances that droplets will coalesce. Drainage and coalescence time are often used interchangeably, even though some authors divide the coalescence time into drainage and rupture times [8]. In dynamic conditions, however, the value of the rupture time is orders of magnitude lower and the difference between the drainage and coalescence time becomes negligible.

Several techniques have been developed to measure the coalescence time, most of them in static conditions, but also a few in dynamic conditions. A spinning drop technique was presented by Flumerfelt et al. [9], where two oil droplets were forced into contact by tilting the capillary. This technique was utilized to determine the coalescence time of crude oil drops in alkaline water at elevated temperatures [10]. In another approach, a pendant drop was used to study the coalescence time between the drop and interface [11, 12]. Two capillaries allowed measuring coalescence time between drops, either based on video analysis [13-15] or measurement of capillary pressure [8, 16]. These methods allowed some control of the droplet size, approach force and velocity, but the experiments were conducted in static conditions with long measurement times. More recently, high-speed imaging was used to study coalescence in dynamic conditions. Kamp and Kraume [17], Villvock et al. [18] and Gebauer et al. [19] developed a cell for binary drop coalescence investigations during flow. A high-speed camera was also used by Luo et al. [20] to study the coalescence of crude oil droplets dispersed in alkali-surfactant-polymer solutions.

Many of the aforementioned methods require the use of quite large (>1 mm) drops, which is often irrelevant for industrial applications. It can also take long time (hours or days) to obtain the number of measurements required for statistically valid results. By contrast,

microfluidics combines control of the experimental environment and dynamic conditions, and at the same time significantly reduces measurement times. Microfluidics allows precise control over fluids in micron-sized channels and, when coupled with high-speed imaging, allows visual observations of hundreds of coalescence events between micron-sized droplets during flow. Many advances have been made since Bremond and Bibette summarized the possibilities of microfluidics in emulsion science [21]. Krebs et al. introduced [22] and utilized [23] a microfluidic collision channel for studying coalescence times for a series of mineral and silicone oils, mostly focusing on their viscosities and resulting changes in capillary numbers. Recently, their results were used to model coalescence kinetics with population balance equations [24]. Film drainage in water-in-oil Pickering emulsions was studied by Zhou et al., who invoked one-to-one collisions between particle-covered droplets [25]. Liu et al. investigated the effect of the intersection angle [26] and shape [27] of modified T-junctions on the coalescence of water droplets, dispersed in silicone or paraffin oil. Coalescence time of gas bubbles in water containing various sodium halides was studied by Wang et al. [28]. Nowbahar et al. reported a microfluidic device for studying destabilization of water-in-diluted bitumen emulsions after adding a de-emulsifier [29]. The measurements were performed in a long serpentine channel without flow, and the coalescence times were two-three orders of magnitude longer than in the previously cited literature. Lin et al. used a collision chamber to investigate coalescence of asphaltene stabilized water-in-oil emulsions in the presence of de-emulsifiers [30], however, they focused on comparing coalescence rates, rather than coalescence times. Finally, a recent paper by Wang et al. presented the effect of dissolved oxygen on coalescence kinetics of squalene droplets in water [31]. While the experimental approach is similar to the one presented here, they reported coalescence of only one size class of droplets with far less coalescence times detected. While some authors

performed experimental measurements of contact time between single droplets or bubbles [18, 32], to the best of our knowledge, no papers involving microfluidic methods have reported contact time measurements.

In the present study we report a novel microfluidic chip design to investigate interactions between micron-sized oil drops in water. Thousands of collision and coalescence events in dynamic conditions were recorded in seconds-long image series. Our approach allows for simultaneous determination of coalescence times of different drop sizes. In addition, it was possible to extract information about the contact time and droplet approach velocity. The method was verified by systematic variations of water salinity, oil composition, concentration of surfactant and temperature. This allowed for comparison with theoretical principles and available experimental data on coalescence time.

2. MATERIALS AND METHODS

2.1. Chemicals

If not stated otherwise, all chemicals used in this study were of analytical grade. Heptane, dodecane and xylene were used as the dispersed phase. The physical and interfacial properties of the oil phases are listed in Table 1. Density was measured with DMA 5000 M laboratory density meter (Anton Paar, Austria), while viscosity with MCR 301 laboratory rheometer (Anton Paar, Austria). Interfacial tension measurements were performed with Sigma 70 Du Noüy ring tensiometer (KSV, Finland). Span®85 was added to xylene in some of the experiments and the interfacial tensions between these phases were measured with SVT20 spinning drop tensiometer (DataPhysics Instruments, Germany). Aqueous solutions were prepared with deionized water (Millipore Simplicity Systems, Germany) with exception

of distilled water in the Salinity section. The low salinity solution was prepared with 0.12 % wt. NaCl, whereas the high salinity solution contained 3.5% wt. NaCl.

Table 1 Properties of the oil phases.

Oil phase	Density @20°C [g/cm^3]	Viscosity @20°C [mPa*s]	IFT in 3.5% wt. NaCl @22°C [mN/m]
Dodecane	0.75	1.51	49.2
Heptane	0.68	0.55	47.4
Xylene	0.87	0.54	38.2

2.2. Microfluidic chips and setup

Custom-designed glass microfluidic chips (Figure 1) were manufactured by Micronit Microtechnologies B.V. (The Netherlands). The inlet channels for oil and water phases were 100 µm wide and lead to a T-junction where the droplets were generated. After passing through a meandering channel, the droplets entered a 500 µm chamber and were split into two streams, which lead to a square (3 mm x 3 mm) chamber where the recordings were taken. All sections had a uniform depth of 45 µm. The droplets were split into two streams in order to minimize the coalescence before entering the square channel. After entering the coalescence channel, the droplets could undergo one or more coalescence events. After each experiment, the chips were sonicated for 15 min in the following solutions: 2% aq. solution of Decon 90™, isopropanol and deionized water. Afterwards, they were dried and baked in an ashing furnace for 6 hours at 450°C to remove all organic components remaining in the channels after experiments and cleaning. Prior to each experiment, the chips were treated in an oxygen plasma chamber (Zepto, Diener electronic GmbH, Germany) for 10 min to increase their hydrophilicity and remove any leftover contaminants.

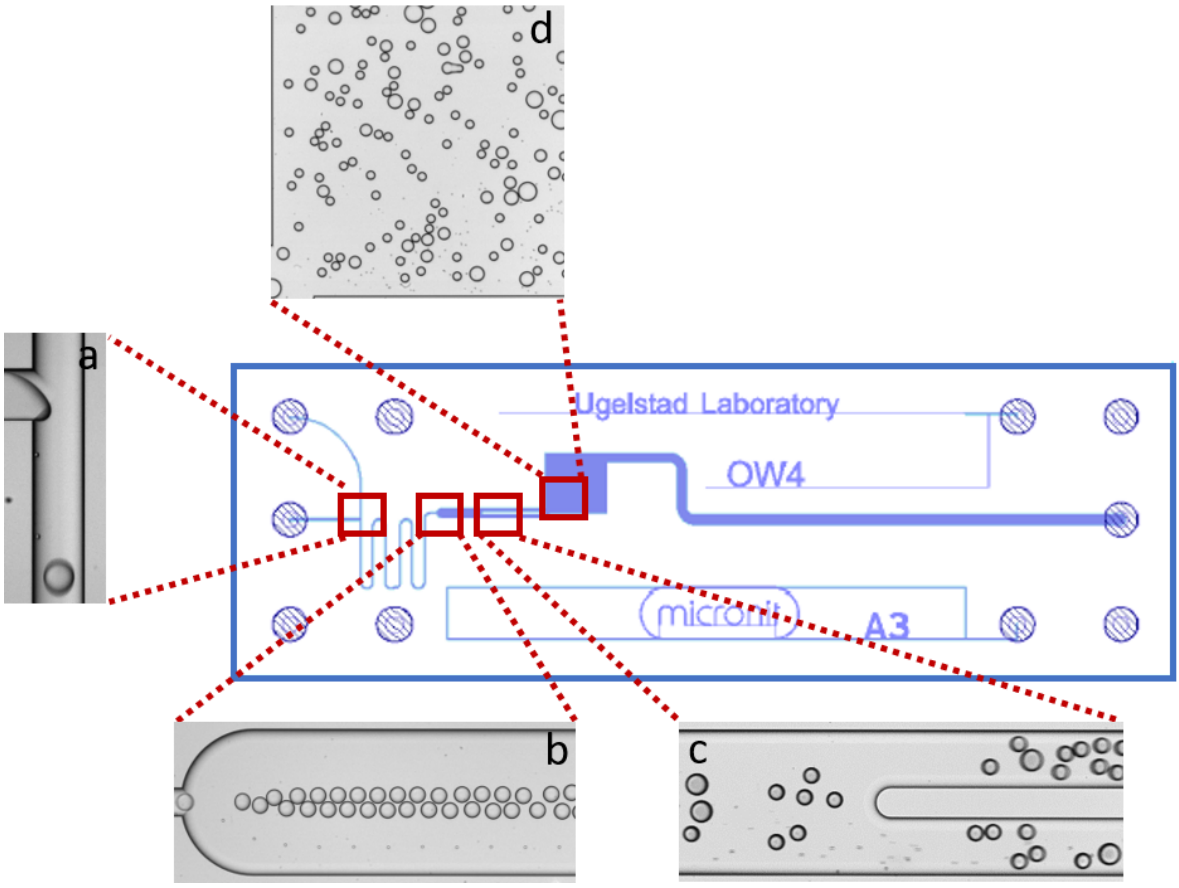

Figure 1 Design of the microfluidic chip. Insets show specific parts of the device. Drops are generated in a T-junction (a) and flow through a meandering channel to wider channel (b). The channel is split into two (c) to minimize coalescence of drops before entering the coalescence chamber (square channel – d), were the coalescence time measurements were taken.

A Fluidic Connect PRO chip holder (Micronit Microtechnologies, B.V., The Netherlands) was used to connect the flow setup to the chip in most experiments (not in the temperature-controlled measurements, see Figure S1 and description in SI). The liquids were pumped with syringe pumps (neMESYS, Cetoni GmbH, Germany) equipped with glass syringes. The flow rate of the water phase was kept constant at 160 µl/min, whereas the flow of the dispersed phase ranged between 5 and 8 µl/min. This variation of the flow minimized coalescence before entering the square channel, since the extent of coalescence differed between the studied systems. Even though some droplets coalesced before entering the square channel, the majority of droplets were of the initial size. In any case, the custom-written Matlab script allowed to filter out the coalescence between droplets of specific sizes, as described later. The average droplet velocity in the square channel was ca. 1.5

cm/s. During the method development stage, it was determined that the number of droplets in the square channel (controlled by the flow rate of the dispersed phase) affected the contact time and number of coalescence events, but not the coalescence time. Due to variations in the chemical properties of the dispersed phase and the type and concentration of surfactants, the initial drop size ranged between 55 and 60 μm in diameter, but was the same for a given system. The experiments were recorded with a high-speed camera (AX100, Photron, Japan), connected to an inverted microscope (Ti-U Eclipse, Nikon, Japan) using a magnification of 6x (4x objective and 1.5x intermediate magnification). Lower magnification was not possible due to insufficient quality of the captured images, which constrained the data analysis.

Each experiment consisted of three parallels and six recordings per parallel. The recordings were captured at 13 600 frames per second for 3.21 seconds (43 674 frames total) with the shutter speed set to 1/50000 s. The resolution was 512x512 pixels. The frame captured approximately 25% of the total area of the coalescence chamber (lower left corner of the square channel in Figure 1).

2.3. Data analysis

The recorded series of images were imported to ImageJ. First, they were converted to binary images and then batch-processed with the use of the Analyse Particle feature. This allowed detection of all the objects in each of the frames and describe them with the following parameters: area, XY coordinates of the centre of mass and shape descriptors – circularity (*circ*), aspect ratio (*AR*) and roundness (*rou*). One frame could contain up to 150 objects, meaning that there could be more than 6 million objects in a single recording. The data was saved as a text file and imported to a purpose-made Matlab script, where the

evaluation of the coalescence times between droplets was carried out in the following steps:

Identification of coalescence events

First, a shape parameter (P_s) was calculated for each of the detected objects with Equation 1:

$$P_s = \frac{\sqrt{AR}}{rou^3 * circ} \quad (1)$$

For individual droplets, all the shape descriptors, and therefore the shape parameter, were close to 1. For coalescing objects (red-framed inset in Figure 2), the value of the shape parameter was larger than 1. Typical values of shape descriptors for coalescing objects were as follow: *AR* >2, *rou* <0.7, *circ* <0.7, thus P_s being larger than 5.

Mapping of drop trajectories prior to coalescence

Once a coalescing object was detected, the coalescence frame number, the coordinates of the coalescence and the size of the final droplet were recorded. Then, the XY coordinates of the two droplets forming the coalesced object were retrieved in all the frames leading up to the detected coalescence event. In this way, the distance between the drops was determined. Figure 2 shows the outcome of the droplet tracking, which shows both the approach of droplets (blue to green) and film drainage (yellow to red).

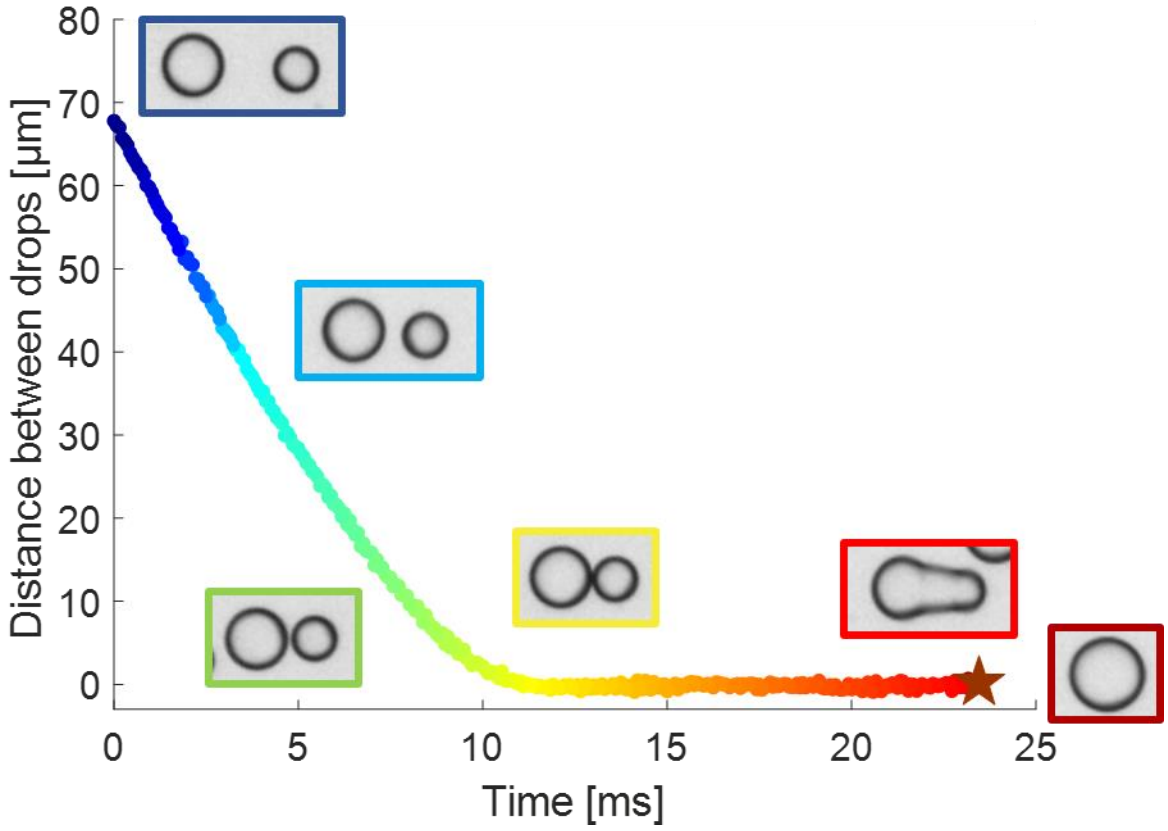

Figure 2 Distance between surfaces of two to-be-coalesced droplets as a function of time.

Detection of onset of film drainage

The next step was to detect the moment when the droplets first came into contact, which we define as the onset of the film drainage. As pointed out by Krebs et al. [22, 23], in this size range the liquid film surrounding the droplets is in the range of tens of nm, and the change in its thickness cannot be followed by microscopes with standard magnification. Therefore, it was defined that the drainage time started in the first frame, where the distance between the two (to-be-coalesced) droplets was below 1 µm. Choosing a smaller value could have led to an incorrect detection of that frame, as the calculated distance between the centres of masses varied slightly, when droplets were in contact.

Estimating coalescence times

Inset with red frame in Figure 2 shows two droplets, immediately after the film rupture. In our (dynamic) system the rupture was incomparably faster than the drainage (some of our initial tests showed this value to be below 10 μs), therefore in this work coalescence time and drainage time will be used interchangeably.

The coalescence time was calculated by subtracting the frame number of coalescence from frame number of first contact, and dividing by the framerate speed of the recording. For the case shown in Figure 2, the coalescence time was 13.2 ms. The methodical error of this approach is estimated to be in the range of ±5 frames (0.37 ms): ±2 frames for the coalescence detection moment, ±2 frames for the first contact detection and ±1 for the framerate speed of the camera. The above procedure was carried out for all the detected coalescing objects, typically 500-1000 per recording. Hence, one parallel contained at least 3000 (and up to 6000) coalescence events. The total number of acquired coalescence time in this paper was over 150 000 for the total recorded footage time of ca. 15 min.

The steps above allow to filter out coalescence between droplet pairs of specific sizes. For clarity, we use size classes instead of actual drop sizes (examples of sizes with respective size classes are provided in Table 2). All newly generated droplets had the same initial size upon generation and were defined as size class 1. If two such droplets coalesce, they form a droplet of size class 2. This droplet can then merge with another droplet of size class 1, forming a droplet of size class 3. A size class is therefore a sum of positive integers, representing the size class of the two droplets forming it. This means that a droplet of size class 4 can be formed both from two droplets of size class 2, or from droplets of size class 3 and 1. Obviously, higher size classes have more possible combinations. However, our

analyses were limited to interactions between droplets of maximum size class 4, since less coalescence events were detected above that class.

Table 2 Droplet diameters of different size classes.

	Droplet diameter [µm]			
	Size class 1	Size class 2	Size class 3	Size class 4
Dodecane	59	80	101	122
Heptane	61	84	104	128
Xylene	60	82	103	126

Lognormal distributions were fitted to each of the experimental datasets obtained from the Matlab script, typically based on a few thousand measured coalescence times. Probability density functions were then plotted based on the mean and standard deviation parameters from the fitted lognormal distributions (Figure 3). In this paper, the terms 'lognormal distribution' and 'probability density function' will be used interchangeably, as all probability density functions had a lognormal shape.

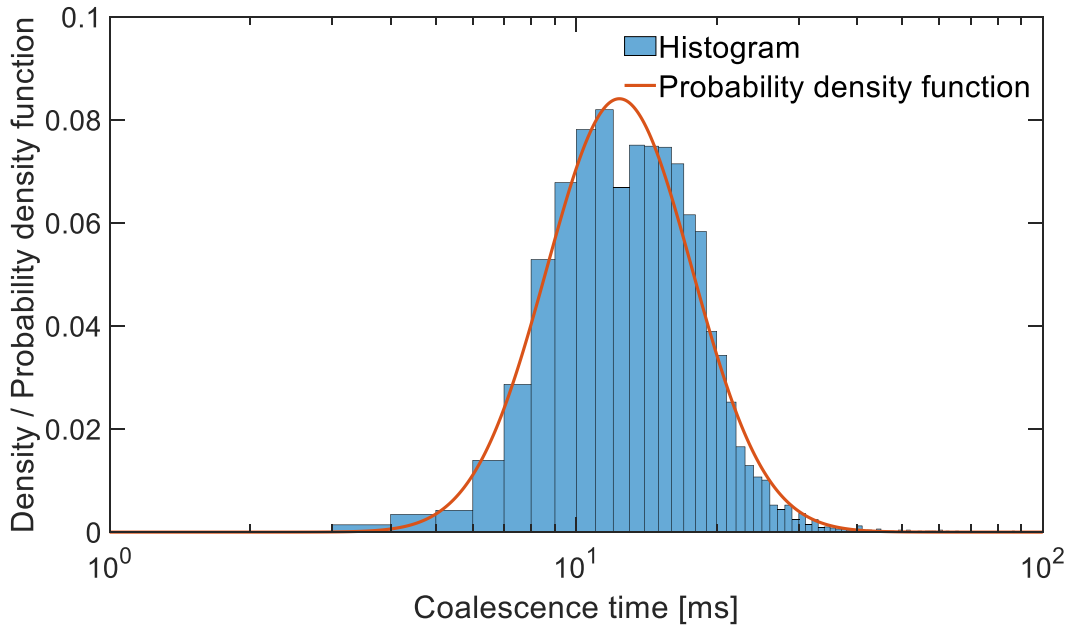

Figure 3 Histogram based on the data from one parallel (bars) and the probability density function fitted to the data (line). Data was divided into 1 ms bins.

In a lognormal distribution, the logarithm of the variable is normally distributed. Thus, when viewing such distributions, the actual values of the left tail of the distribution are several orders of magnitude lower than the actual values of the right tail. In turn, the mean and the variance of the distribution are not ideally suited for describing data of this nature. Unlike in a normal distribution, the mean value is not the most prevalent value, i.e., the value with the largest probability density. The latter value is referred to as the mode, which is smaller than the mean due to the difference in magnitude of the two tails of the distribution.

In order to discuss the trends in the experiments, the values of the modes are used. A trend in the value of the mode means that there is a trend in the most prevalent value. Additionally, a trend in mode is expected to be present in the mean value as well. If the mode and width of two distributions are similar, their probability density functions will almost overlap or overlap. In such cases it should be noted that a shift to the right corresponds to a larger difference then a similar shift to the left, due to the lognormal nature of the plot.

Typical reproducibility for three parallel measurements is shown in Figure S2 in SI. The functions from each parallel were largely overlapping, so for clarity all subsequent distributions were made by combining the data from all three parallels of one experimental condition (usually in the range of 9-12 thousand individual coalescence times in the combined dataset).

Determination of approach velocity

The tracking of droplets also allowed to determine their positions prior to the coalescence event. Therefore, it was possible to calculate the approach velocity between the two to-be-coalesced droplets. This was done by dividing the distance in the 40^{th} frame before first

contact over the time-equivalent of 40 frames (with our framerate, 2.94 ms). The analysis of the effect of approach velocity on the coalescence time solely included the coalescence events between size class 1 droplets.

Determination of contact time

In the present paper, we define contact time as the time the droplets spend in proximity to one another, which does not lead to coalescence. Evaluation of the contact time between droplets was performed with a different approach. The analysis started with detecting a droplet entering the square channel (bottom left corner of inset d in Figure 1). Then the droplet was tracked over the next hundreds of frames (similar method as described above) until it coalesced with another droplet or went out of the field of view. The coordinates of the droplet in each frame leading to either of the events were then saved. The next step was to find the closest droplet in each of the frames, by using the coordinates data. Exemplary results of the analysis are presented in Figure 4.

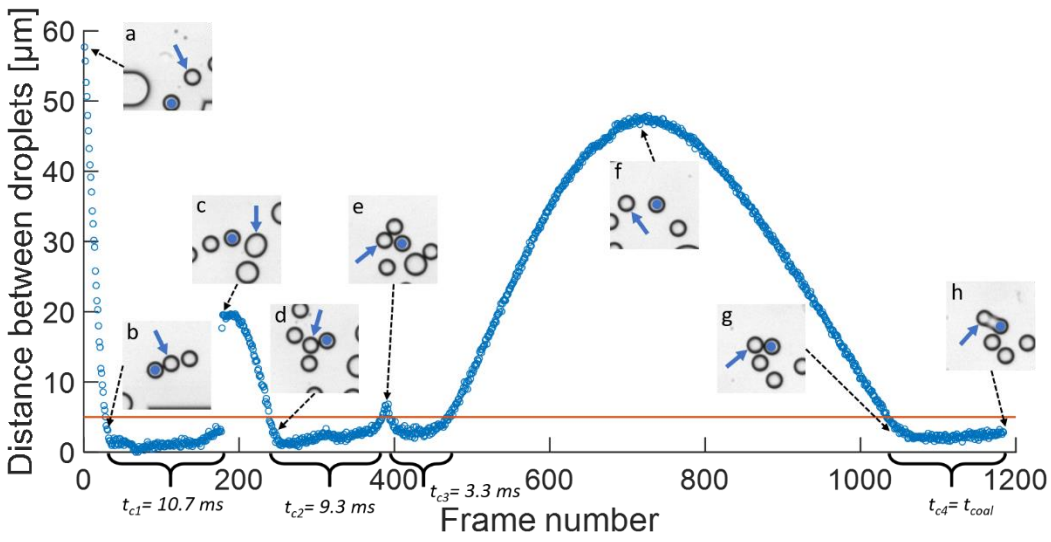

Figure 4 Visual representation of the contact time calculation. Tracked droplet is marked with a filled circle, the other (closest) drop is marked with an arrow.

Here the separation distance between the original drop (filled circle) and any other closest droplet (arrow) was plotted against the frame number. When entering the channel, the initially large separation distance (inset a) quickly decreased (inset b). The droplets stayed in contact (first measured contact time), until it was interrupted by a coalescence between nearby droplets (inset c) and the distance increased momentarily. Later, the original droplet got in contact with two other droplets (insets d and e), which allowed detection of the second and third contact time. After detaching, the droplet flowed separately for some time (inset f) and finally collided with the droplet it eventually coalesced with (insets g and h).

Every time the distance between droplets was below 5 μm value (the orange solid line) and stayed below it for at least 14 consecutive frames (ca. 1 ms), the contact time was recorded. The contact times leading to coalescence between drops were not included in these datasets. Only the size class 1 droplets were taken into consideration when entering the square channel. Similar to the coalescence times, lognormal distributions were fitted to the data and the results were presented as probability density functions. Contact time evaluation was only performed on the systems with the same dispersed flow rate, as lower/higher number of drops could affect the results.

3. RESULTS AND DISCUSSION

Five parameters were investigated one at the time to demonstrate the versality of the developed microfluidic tool: salinity of the water phase, oil phase composition, droplet size, concentration of an oil-soluble surfactant and temperature. Lastly, we analysed the effect of approach velocity on the coalescence and contact times.

3.1. Salinity

Figure S3 in SI illustrates the impact of salinity on the droplet size inside the coalescence chamber. Little coalescence was observed in distilled water. Merging between droplets notably increased when some electrolyte was added to the solution, whereas it was quite extensive in the high salinity solution.

An important aspect of these observations was a distinction between the sizes of coalescing droplets. It was observed that in distilled water the majority of coalescence was between droplets of initial size, whereas a lot of merging was also detected for larger droplets when salinity increased. It greatly influenced the coalescence time distribution when all merging events were taken into account (Figure S4 in SI). For this reason, it was useful to extract and distinguish the coalescence times of different size classes. In this section, however, we consider only the coalescence times between droplets of initial size, and use it to illustrate the interpretation of the distributions. The expansion into coalescence times for different drop sizes is shown in the next section.

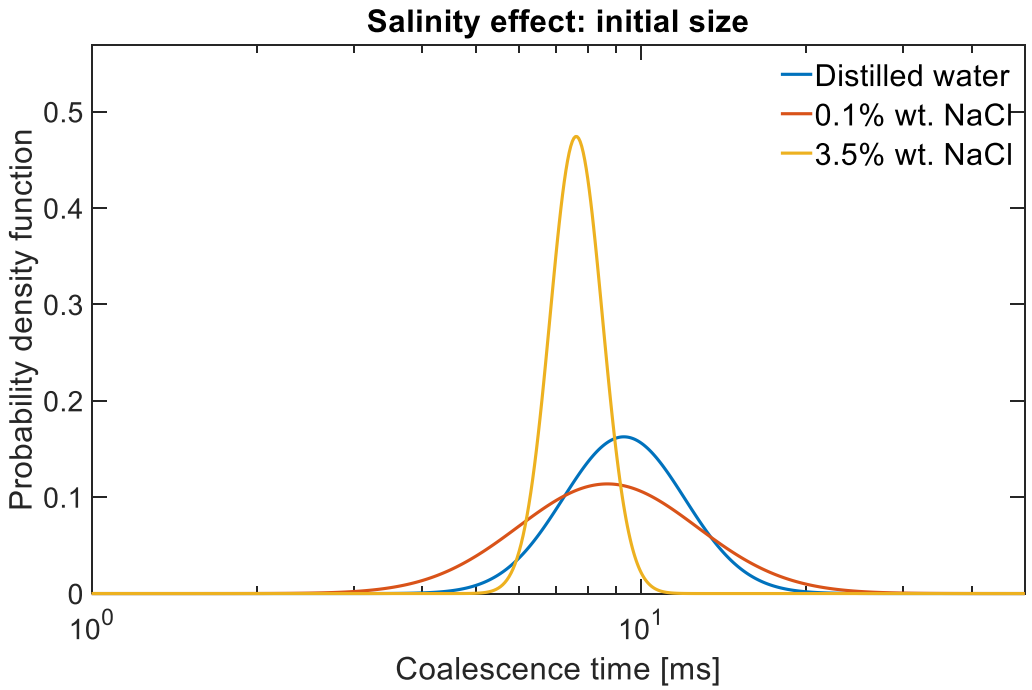

Figure 5 Coalescence time distributions of initial-sized xylene drops in distilled water, low salinity and high salinity brines.

The coalescence time distributions for xylene droplets in the solutions with different salinities are shown in Figure 5. Two important aspects can be deduced from the curves: 1) The location of the maximum (i.e. mode) on the x-axis, where the coalescence times are shorter when the mode is shifted to the left; 2) the width of the distributions, which shows the range of observed coalescence times. The shortest coalescence time (7.6 ms, based on the mode) was observed for the 3.5% wt. brine, i.e. high salinity. Also the obtained coalescence times were the least spread at the highest salinity, as more than 95% of the values were found to be between 5 and 11 ms. Coalescence in the low salinity brine (0.1% wt. NaCl) had the widest distribution of coalescence times – ranging from 3 to 30 ms, with the mode at 8.6 ms. The longest coalescence times were obtained in the distilled water, with the mode equal to 9.3 ms.

It is well known that oil drops acquire a high negative charge in aqueous solutions [33]. In the case of distilled water, the extension of the electrical double layer is large. When considering the electrolyte concentration, the Debye length in this water phase would

probably be in the range of 300 nm, which is considerably more than the thickness of the thin film separating the droplets [34]. Adding an electrolyte to the solution leads to screening of the negative charge by adsorption of cations and anions in the diffuse layer, which effectively reduces the extent of the electrical double layer and the repulsive forces. When adding the sodium chloride in our system, the Debye length is effectively reduced to ca. 2.2 nm and 0.4 nm for the low and high salinity solution, respectively. This means that the electrostatic forces are weak at larger separation distances and can explain the decreased coalescence time and increased coalescence rate between drops. The extent of the electrostatic repulsion can also explain the difference in the width of the coalescence time distributions when comparing the high salinity solution with the other two. In the former, the probability of collision is almost solely dictated by the hydrodynamic conditions, whereas in the latter the long-ranged electrostatic repulsion cannot be neglected. Therefore, the collision force could vary quite significantly, which in the end affects the length of film drainage.

3.2. Oil phase and drop size

The benefits of extracting the coalescence times for different size classes are outlined in this section. The coalescence times for all droplet sizes of three different oil phases in high salinity brine are shown in Figure S5 in SI. The high salinity conditions ensured merging of droplets of many size classes.

The coalescence times for heptane and xylene were 9.5 ms and 9.9 ms, respectively. For dodecane the range was broader with the mode at 11.8 ms. More details could be extracted from the data by dividing the coalescence times into individual size classes. This is shown for xylene drops in Figure 6.

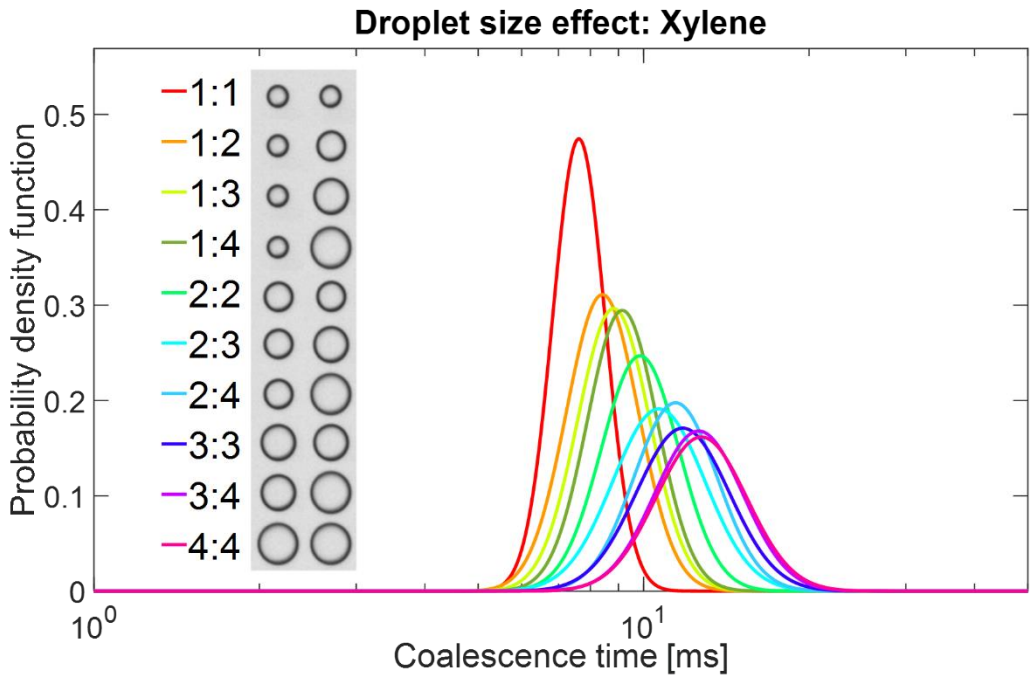

Figure 6 Coalescence time distributions of xylene droplets in high salinity brine, divided by the droplet size classes taking part in a coalescence event. 1:1 relates to coalescence of two droplets of size class 1, 1:2 to coalescence between droplet of size class 1 and 2, etc.

The coalescence time was shortest for two droplets of the initial size class (1:1). The larger the droplets, the longer time was required for the film to drain. What is more, when a droplet could be formed in two ways, e.g. a droplet of size class 4 could be a result of 1:3 or 2:2 merging, the coalescence was typically shorter when a smaller droplet was involved. Similar observations were made for heptane and dodecane (Figure S6 and S7 in SI, respectively).

When the coalescing droplets are not of even size, it is usual for modelling purposes to calculate the diameter equivalent (d_{eq}) with the following equation (Equation 2) [4]:

$$d_{eq} = \frac{2 * d_1 d_2}{d_1 + d_2} \quad (2)$$

where d_1 and d_2 are the diameters of the coalescing droplets. The diameter equivalents for all the size classes (Table 2) were plotted against the modes of coalescence time distributions in Figure 7.

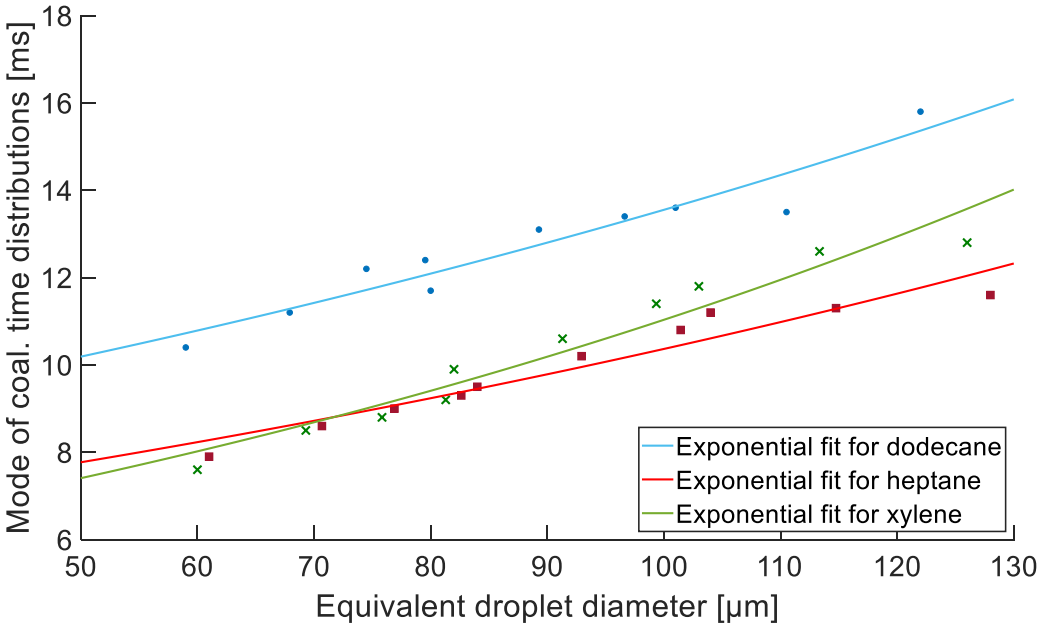

Figure 7 Modes of coalescence times distributions for dodecane, heptane and xylene droplets plotted against the equivalent droplet size involved in coalescence. Solid lines show modelled results, based on Equation 4.

The dodecane drops had noticeably longer coalescence times than the other oils. The droplets of heptane and xylene had similar drainage time at lower equivalent diameters, but a difference emerged at larger drop sizes. It should be noted that when the final droplet could be formed in more than one way, d_{eq} will always be lower in the coalescence event involving a smaller droplet i.e. it will be ca. 75 and 82 µm for 1:3 and 2:2, respectively.

Chesters presented several coalescence models for droplets depending on the rigidity and mobility of the involved interfaces [4]. Typically, the drainage time is a function of the viscosity of the continuous and (less often) dispersed phases, interfacial tension, initial and critical film thickness, interaction force and the droplet size. The droplet size is probably the most important parameter, and its exponent frequently varies between 1.5 and 2. Here we use the simplest expression for drainage time (t_{dr}), defined for the coalescence between non-deformable, unequal sized particles d_1 and d_2 (Equation 3):

$$t_{dr} = \frac{3\pi\mu_c}{2F} * \left(\frac{d_1 d_2}{d_1 + d_2}\right)^2 * ln\left(\frac{h_i}{h_f}\right) \quad (3)$$

where μ_c is the viscosity of the continuous phase, F is the interaction force, and h_i and h_f are the initial and critical film thickness, respectively. The interaction force [4] and both film thicknesses [35] will to some extent depend on the droplet diameter, but for simplicity we considered these parameters to be constant. Therefore, Equation 3 can be approximated to the following (Equation 4):

$$t_{dr} \approx const * \left(\frac{d_1 d_2}{d_1 + d_2}\right)^2 \quad (4)$$

This model was fitted to the modes of coalescence time and equivalent diameters, shown as the solid lines in Figure 7. The fits are satisfactory, with all coefficients of determinations above 0.9, meaning the results are in line with the theoretical considerations. Physically, the longer drainage times for larger droplets was attributed to larger volumes of the continuous phase to be drained prior coalescence. Similarly, during the formation of droplet of the same size (e.g. drop of size class 4 formed out of size classes 1:3 or 2:2), the event involving a smaller droplet was typically quicker. In this situation, the interface of the smaller droplet is probably less likely to deform, resulting in less thin film volume to be drained.

In the case of dodecane, the coalescence time was considerably longer than the other two oils, even though this oil phase has the highest Hamaker constant [36] and is considered more hydrophobic (partition coefficients – log K_{OW} – of 6.1, compared to 4.7 and 3.2 for heptane and xylene, respectively), both of which would lead to an increase of the attraction between the colliding drops. Most likely the increased viscosity of dodecane, also decreasing the interfacial mobility, led to an increase of coalescence time as suggested by other authors [23, 37]. By comparison, Wang et al. reported the coalescence time of squalene droplets (eight

times the viscosity of dodecane) in the range of 15-60 ms, depending on the concentration of dissolved oxygen [31]. Krebs et al. also reported longer coalescence times for increasing viscosities of mineral and silicone oils [23]. Although the droplets generated in our microfluidic device should be small enough to be considered as non-deformable and rigid particles [5], it is quite clear that even at this scale the viscosity of the dispersed phase will have an effect on the drainage time.

In our previous work we also studied heptane and xylene systems in similar conditions, although using a different microfluidic chip design [38]. There we found a small difference between coalescence times of heptane and xylene, which was attributed to the stronger adhesive forces between the aromatic π-electrons in xylene and surrounding water molecules that decreased the oil-water interfacial tension and slightly prolonged the drainage time. Furthermore, additional hydrophobic attraction, arising (amongst other things) from the presence of dissolved gas molecules at the interface, could also have contributed to the lower coalescence time of heptane. The results presented in this work are based on a significantly larger number of coalescence events, and therefore are more statistically relevant. What is more, we are now able to distinguish the coalescence between droplets of different sizes. Although the coalescence time distributions including all droplet sizes (Figure S5 in SI) hardly show any difference between heptane and xylene, Figure 7 shows that when the drop size increased, heptane drops coalesced faster. This means that more information about the coalescence times can be revealed. As previously [38], we can use the expression for the total interaction energy between two spherical particles, given by Equation 5, to discuss this variation:

$$V_S(kT) = \frac{R}{kT}\left[2\pi\epsilon_0\epsilon\psi_0^2 exp(-\kappa H) - \frac{A_{121}}{12H} - A_1 exp\left(-\frac{H}{\lambda_1}\right) - A_2 exp\left(-\frac{H}{\lambda_2}\right)\right] \quad (5)$$

where V_S is the total interaction energy between spheres in kT units, R is the spherical droplet radius, $\epsilon_0\epsilon$ is the permittivity of water, ψ_0 is the particle's electrostatic potential, κ^{-1} is the Debye length, H is the distance between the droplet surfaces and A_{121} is the Hamaker constant. The values of A_1, A_2 (constants) and λ_1, λ_2 (decay lengths) are usually experimentally determined. The first term inside the square brackets describes the electrostatic repulsion, which for our system can be neglected due to high electrolyte concentration. The next term represents the van der Waals forces, whereas the last two account for the hydrophobic interactions. In our case, the interaction energy depends on the chemical properties of the oil phase and the size of the droplet. When smaller droplets are considered, the difference between the net interaction energy of the two systems is probably negligible. However, with the increase of the droplet size, the contribution from the hydrophobic interactions becomes more significant, which could explain why the coalescence of bigger heptane droplets proceeded faster than those made out of xylene.

3.3. Oil-soluble surfactant

The coalescence time distributions of xylene droplets with different concentrations of an oil-soluble surfactant (Span®85) are shown in Figure 8. For clarity, only the initial size droplets were considered.

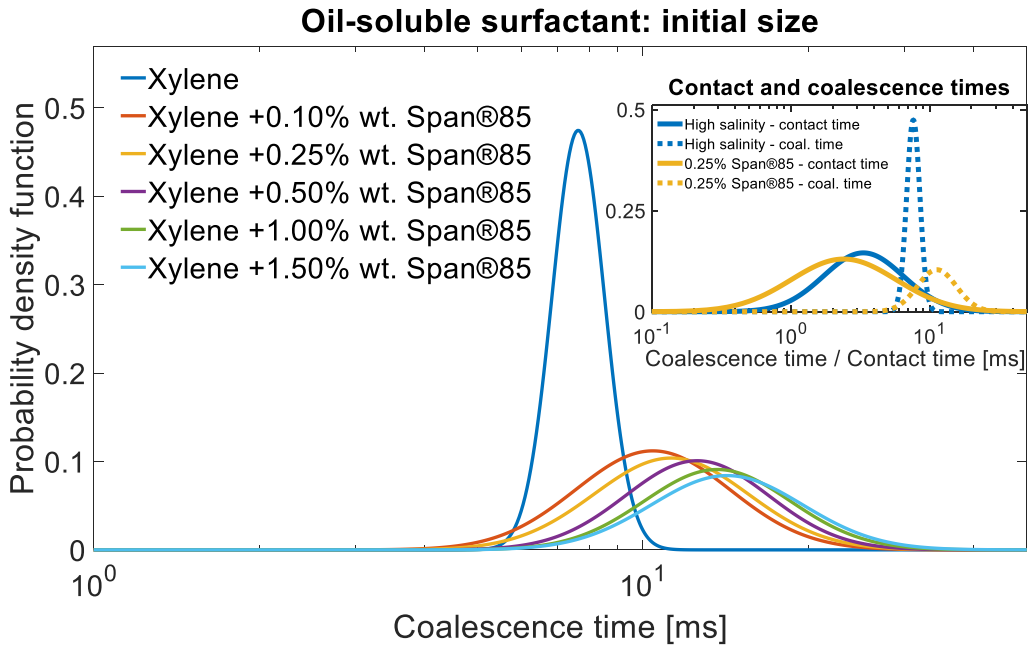

Figure 8 Coalescence time distributions of initial-sized xylene with and without oil-soluble surfactant in high salinity brine. Inset shows comparison between contact and coalescence times in systems with and without surfactant.

Clearly, the addition of surfactant to the oil phase increased the coalescence time, and the mode increased from 7.6 ms for pure xylene to 10.5 ms with the lowest concentration of Span®85. With increasing concentration of surfactant in the oil phase, there was a gradual shift towards longer coalescence times, accompanied by wider distributions. The average contact time was, however, found to be shorter with the surfactant than without, as seen from the inset in Figure 8.

The effect of the surfactant was illustrated in another way in Figure 9, where the duration of coalescence events (coloured dots) between initial-sized droplets was plotted as a function of the position of the detected film rupture in the channel.

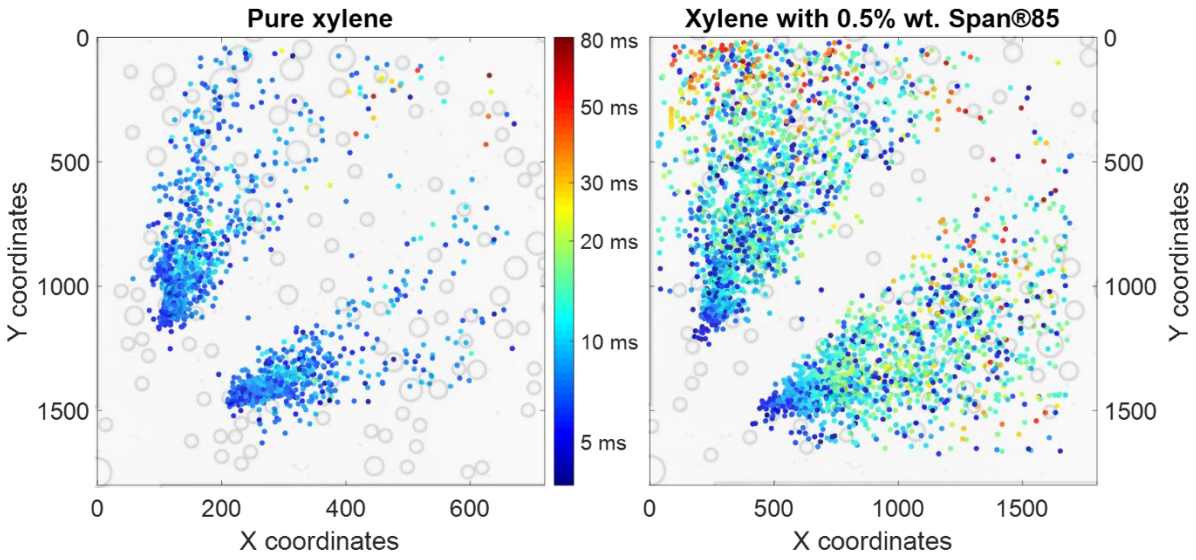

Figure 9 Coordinates of the detected coalescence events in high salinity brine without (left) and with an oil-soluble surfactant (right) with their respective duration, represented by the colour of the dot in the scatter plots.

Two main differences were noted with and without the surfactant dissolved in the oil phase. Firstly, the great majority of coalescence events between droplets made of pure xylene were shorter than 15 ms (mostly blue-coloured dots), while the coalescence took significantly longer after adding the surfactant. The effect of surfactants on the coalescence of emulsion droplets has been extensively studied for decades and is well understood [39, 40]. In general, the surface-active molecules adsorb at the oil-water interface and influence the interfacial properties (interfacial tension and elasticity). The values of interfacial tension (IFT) in the systems with Span®85 are presented in Table 3.

Table 3 Interfacial tension of xylene with and without oil-soluble surfactant against high-salinity brine.

Concentration of Span®85 [% wt.]	0	0.10	0.25	0.50	1.00	1.50
Interfacial tension [mN/m]	38.2 ±0.1	30.4 ±0.4	17.3 ±1.1	10.0 ±0.6	7.9 ±1.3	6.0 ±0.9

As expected, the IFT values decrease with the increasing surfactant concentration. Adsorption of non-ionic surfactants, such as Span®85, can also provide steric repulsion

between oil droplets. This is often a combination of unfavourable mixing of the hydrophilic groups and volume (steric) restrictions during approach of droplets. This could have also influenced the shorter contact times between the droplets. As noted by Muilwijk et al., when surfactants are present in the dispersed phase, their transport is driven by the continuous phase flow (constant in our system) and also depends on the dispersed phase viscosity [41]. Adding Span®85 might in fact increase the viscosity of xylene and decrease the convective mass transfer of surfactant molecules to the interface. However, the more dominant effect probably resulted from the higher concentration of surfactant inside the droplets. As seen from the IFT values in Table 3, increasing the concentration of Span®85 above 0.5 % wt. does not result in as dramatic decrease of IFT as below that value. This suggests that at this point the interface could already be saturated and higher concentration of surfactant in the oil phase will simply lead to faster coverage of the surface. In addition, the Marangoni effect can occur, where the concentration gradient of surfactants is formed due to the flow of fluid close to the interface upon collisions between drops [2]. This gradient causes local changes in the interfacial tension, which can create a flux in the opposite direction of the film drainage, increasing the time of coalescence.

Second major difference concerns the location of the coalescence events inside the square channel. Most of the xylene drops coalesced close to the inlet of the channel, which reduced the number of initial-sized droplets available for coalescence further inside the square channel. Conversely, due to increased stability, coalescence of droplets with surfactant was spread more evenly across chamber. It should also be noted that in both cases many shorter coalescence events could be spotted close to the inlet of the channel, however this effect was far more evident for the system with surfactant. In addition, hardly any coalescence

event was observed along the diagonal of the channel, which was caused by the flow patterns arising from the two-inlet chip design of the square channel.

Another interfacial effect that could explain why most of the shortest coalescence events took place at the inlet of the channel is the stagnant cap phenomenon. When droplets are in motion, some of the surfactant molecules can be swept into the stagnant cap region ('end of the drop') [42]. This will decrease the interfacial concentration of the surfactant molecules at the remaining part of the interface and could impact the drainage process. The droplets entering the square channel have approx. 5 times higher velocity than inside it. When the droplets slow down, the relaxation process, driven by the gradient in the interfacial concentration, will immense and result in more even distribution of surfactant molecules at the oil-water interface. This could also explain why the further the droplet travel, the longer the coalescence time seems to be (more yellow, orange and red dots can be seen on the edges of the right image of Figure 9), as there is more time for re-distribution of the surfactant molecules at the interface. It is also possible that newly created oil droplets had not yet reached its equilibrium interfacial tension with the surrounding aqueous phase, due to short residence time and perhaps the kinetics of the surfactant adsorption.

3.4. Temperature

The efficient heat transfer in microfluidic systems was utilized in this section. The fluids pumped to the chip are at room temperature, but can quickly be heated to the temperature of the glass chip due to small dimensions of the device [43]. Therefore, by controlling the temperature of the chip with the use of a custom-made chip holder, it was possible to measure the coalescence time of oil drops in temperatures up to 50°C. The modes of the probability density functions (Figure S8 in SI) are presented in Table 4.

Table 4 Modes of coalescence time distributions of merging events performed at different temperatures.

Temperature	23°C	30°C	40°C	50°C
Coalescence time mode [ms]	13.7	10.1	8.8	6.7

The results are based on the coalescence of initial-sized xylene drops with 1% wt. Span®85 in high salinity brine. A system with surfactant was chosen as the merging at high temperatures was extensive and some initial stability was necessary. As shown in Table 4, the coalescence times steadily decrease from 13.7 ms at room temperature to 6.7 ms at the highest temperature conditions.

Thermal treatment of emulsions is a common method for their destabilization [1]. Higher temperature affects the number of collisions between the droplets, resulting in droplet growth. The temperature increase lowers both the density and viscosity of the oil and water; and especially the latter plays an important role in the drainage process. The viscosity of the continuous phase is often thought to be of greater importance, especially in the numerical considerations [4, 5]. The results presented here agree with other reports, where other methods than microfluidics were used to study the coalescence in higher temperatures [10, 13, 44].

Interestingly, the number of detected coalescence events was similar at all temperatures. This was possibly due to faster film rupture when the temperature was increased. As explained in the Experimental section, our coalescence time measurement method relies on detecting droplets just after film rupture. In room temperature, the film rupture process probably takes less than 10 µs (our previous coalescence time measurements were performed at considerably higher framerates [38] and yet we were not able to make a detailed

recording of a film rupture event). The rupture process was most likely even faster at higher temperature, which lead to lack of detection of some coalescence events.

3.5. Approach velocity

In the last section we present the effect of the approach velocity on the coalescence and contact times. We observed that contact time depends on the number of droplets entering the channel, therefore systems with similar number of generated droplets per unit time were considered for comparison. The results for xylene with 0.1% wt. Span®85 are shown in Figure 10, while other systems (dodecane, pure xylene and xylene with 1% wt. Span®85) are shown in Figures S9-11 in SI.

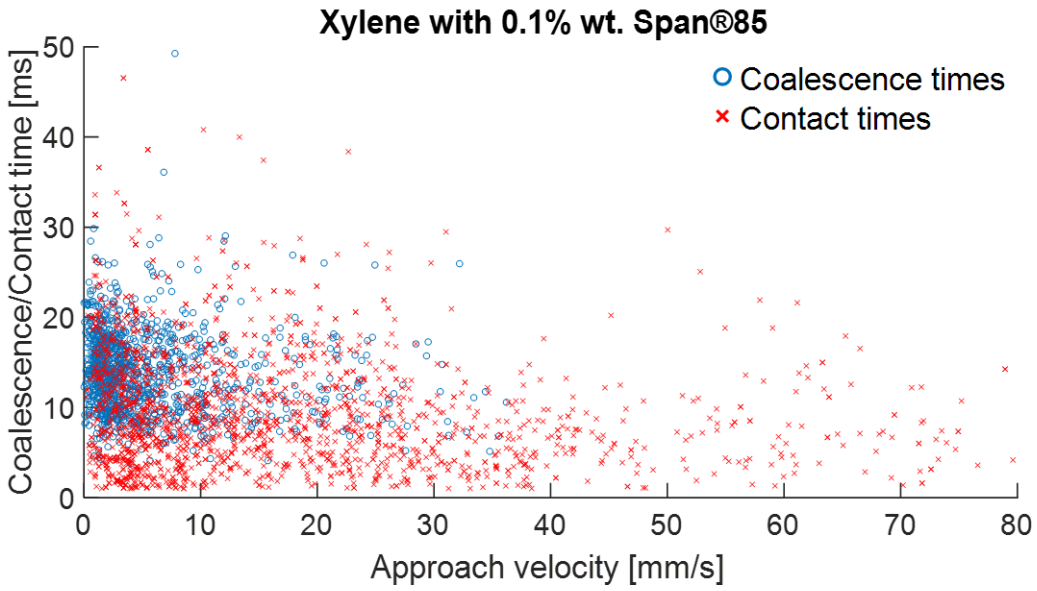

Figure 10 Coalescence and contact times as a function of approach velocity for xylene with 0.1% wt. Span®85. Singular coalescence/contact time events were detected outside of the axis limits but were not shown for clarity and consistency.

Firstly, the distributions of coalescence and contact times in each system are comparable, with one noteworthy difference – a significant share of the detected contact events was shorter than the minimum coalescence time. As outlined in the introduction, in order for the two droplets to coalesce, sufficient time is required for the thin film to be drained. If that time is longer (e.g. xylene with surfactant), many of the collisions will end in contact,

rather than coalescence. Secondly, the effect of the approach velocity on the coalescence time depends on the properties of the oil phase. Xylene had relatively narrow spread of coalescence times (Figure S5 in SI), and the coalescence events were quite evenly distributed up to approach velocities of ca. 30 mm/s. This was not the case for the other oils, were the majority of coalescence events occurred at lower velocities (below 10 mm/s). We also observed that virtually no coalescence took place for velocities higher than 40 mm/s. Thirdly, one could see that the spread of the coalescence and contact times (or the maximum detected values), decrease with the increasing approach velocity. Interestingly, the minimum values of contact and coalescence remain relatively similar over the entire range of the approach velocity.

The coalescence to contact events ratios were classified based on the approach velocity and were plotted in Figure 11.

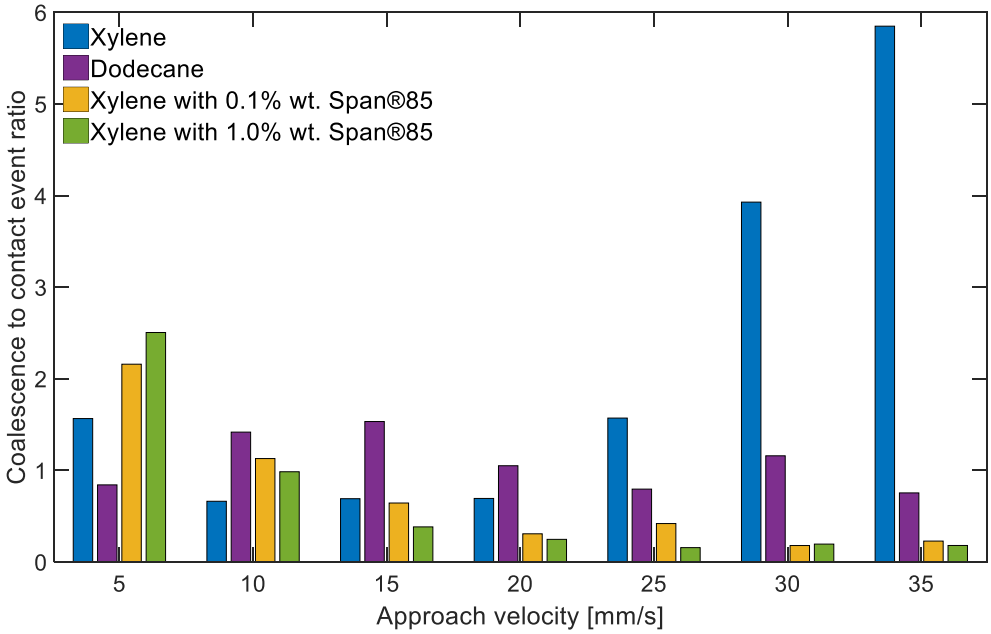

Figure 11 Ratios of coalescence to contact time events classified based on the approach velocity. First bin includes events with velocity up to 5 mm/s, second bin between 5 and 10 mm/s and so on.

This data may give some indication on the likelihood of coalescence in a given system at the specific range of the approach velocity. While dodecane exhibits similar behaviour independent of the approach velocity, xylene drops were more likely to coalesce at higher velocities. Conversely, after adding the surfactant, the trend changes drastically. In both cases, more coalescence than contact events were detected for the two lowest approach velocities.

According to the literature, the effect of the approach velocity on coalescence time is not clear [7], however most reports seem to support the theory that the drainage time should decrease with increasing approach velocity, both for bubbles [7, 32, 45, 46] and droplets [22]. Our data agrees with these results, however we also observe a critical velocity value, above which there is no coalescence. Droplet-droplet collisions can be classified into four regimes with increasing Weber number [47]: (1) coalescence from low-energy collision (minor droplet deformation), (2) bouncing, (3) coalescence from high-energy collision (major droplet deformation) and (4) coalescence from high-energy collision, followed by generation of secondary droplets (splashing). In our system we can probably observe only the two first regimes. It would be reasonable to assume that below the critical value of the approach velocity, the droplets in our system undergo low-energy collisions, while above it they bounce-off. However, it should also be noted that many of the collision events within the suggested low-energy collision range do not end in merging, indicating that are more factors involved (e.g. impact angle [32]) or that coalescence could be more of a stochastic process.

Furthermore, the deformability of the droplets and mobility of the interface should not be neglected. Chesters argued that very small droplets (below 1 mm) should behave as nearly rigid particles [4]. While we did not observe any substantial deformation in any of our systems

(even for bigger droplets), there is a notable difference in coalescence behaviour between the various oil phases, which could be explained by the mobility of the fluid interface. In the case of xylene or dodecane, it can be argued that the interface is non-deformable or deformable with at least partial mobility, which is characteristic for pure liquids with low dispersed phase viscosity, and results in low tangential stress and plug-flow like velocity between the interfaces [48], meaning that the approach velocity should not be an important factor in the drainage process as observed in the case of dodecane. Unfortunately, we could not find an explanation for the results obtained with xylene droplets. On the other hand, the addition of surfactant immobilizes the interface, creating a parabolic drainage velocity profile with no slip at the interface [5], which prolongs the drainage time, as observed here. Similar observations were made with bubble-bubble coalescence [49]. Another effect that can play an important role in the effect of approach velocity on the drainage process is the previously outlined Marangoni effect. In the cases with surfactant, higher velocity could lead to larger displacement of surfactant molecules at the interface upon impact, which would lead to higher interfacial tension gradient. This results in higher Marangoni flux in the opposite direction of the drainage and makes coalescence longer and less likely.

4. CONCLUSIONS

A microfluidic method was developed to study the kinetic aspects of oil droplet coalescence during flow. In contrast to other reported microfluidic methodologies for studying coalescence time, this technique allowed to follow and detect thousands of merging events of different-sized droplets in various conditions with considerably reduced measurement times. What is more, we were able to simultaneously analyze the coalescence times, contact times and approach velocities between the droplets. It was found that the increase of

salinity reduces the coalescence time by decreasing the electrostatic repulsion between negatively charged oil drops. When considering different droplet sizes, larger droplets coalesced slower, independent of the chemical composition of the dispersed phase. This is in line with the theoretical considerations based on the coalescence models found in the literature. The viscosity had probably the largest effect on the coalescence of droplets generated with pure oils. Still, the hydrophobicity of the oil could affect the merging, which was seen for larger droplets. The addition of a surfactant slowed down the kinetics of coalescence – the more surfactant was present, the more the distributions were shifted towards the longer coalescence times. The temperature of the measurements had also a major impact on the drainage time, as the fastest coalescence was observed in the highest temperature. The increase in approach velocity was found to decrease both the coalescence and contact times. A critical approach velocity value was observed, above which no coalescence took place, most likely due to bouncing-off phenomenon. Furthermore, the deformability of droplets and mobility of the interfaces could also play a role in the coalescence process. All the results could be explained with the available literature, which demonstrated the applicability of our microfluidic method for coalescence and contact time measurements.

ACKNOWLEDGMENTS

This work was carried out as a part of SUBPRO, a Research-based Innovation Centre within Subsea Production and Processing. The authors gratefully acknowledge the financial support from SUBPRO, which is financed by the Research Council of Norway, major industry partners and NTNU.

The authors would like to additionally acknowledge the Anders Jahres fond til vitenskapens fremme for providing funding for manufacturing of the temperature control setup, and Marzieh Saadat and Robert Karlsen from NTNU for help with the design and fabrication of the device.

REFERENCES

1. Zolfaghari, R.; Fakhru'l-Razi, A.; Abdullah, L. C.; Elnashaie, S. S. E. H.; Pendashteh, A., Demulsification techniques of water-in-oil and oil-in-water emulsions in petroleum industry. *Sep. Purif. Technol.* **2016,** *170*, 377-407.
2. Tadros, T. F., Emulsion Formation, Stability, and Rheology. In *Emulsion Formation and Stability*, Wiley-VCH Verlag GmbH & Co. KGaA: 2013; pp 1-75.
3. Christenson, H. K.; Claesson, P. M., Direct measurements of the force between hydrophobic surfaces in water. *Adv. Colloid Interface Sci.* **2001,** *91* (3), 391-436.
4. Chesters, A. K., The modelling of coalescence processes in fluid-liquid dispersions: a review of current understanding. *Chem. Eng. Res. Des.* **1991,** *69* (A4), 259-270.
5. Liao, Y.; Lucas, D., A literature review on mechanisms and models for the coalescence process of fluid particles. *Chem. Eng. Sci.* **2010,** *65* (10), 2851-2864.
6. Zhao, H.; Brunsvold, A.; Munkejord, S. T., Transition between coalescence and bouncing of droplets on a deep liquid pool. *Int. J. Multiphase Flow* **2011,** *37* (9), 1109-1119.
7. Orvalho, S.; Ruzicka, M. C.; Olivieri, G.; Marzocchella, A., Bubble coalescence: Effect of bubble approach velocity and liquid viscosity. *Chem. Eng. Sci.* **2015,** *134*, 205-216.
8. Gaweł, B.; Lesaint, C.; Bandyopadhyay, S.; Øye, G., Role of Physicochemical and Interfacial Properties on the Binary Coalescence of Crude Oil Drops in Synthetic Produced Water. *Energy Fuels* **2015,** *29* (2), 512-519.
9. Flumerfelt, R. W.; Catalano, A. B.; Tong, C.-H., On the Coalescence Characteristics of Low Tension Oil-Water-Surfactant Systems. In *Surface Phenomena in Enhanced Oil Recovery*, Shah, D. O., Ed. Springer US: Boston, MA, 1981; pp 571-594.
10. Peru, D. A.; Lorenz, P. B., The Effect of Equilibration Time and Temperature on Drop-Drop Coalescence of Wilmington Crude Oil in a Weakly Alkaline Brine. *Chem. Eng. Commun.* **1989,** *77* (1), 91-114.
11. Kourio, M. J.; Gourdon, C.; Casamatta, G., Study of drop-interface coalescence: Drainage time measurement. *Chemical Engineering & Technology* **1994,** *17* (4), 249-254.
12. He, Y.; Howes, T.; Litster, J. D.; Ko, G. H., Experimental study of drop-interface coalescence in the presence of polymer stabilisers. *Colloids Surf. Physicochem. Eng. Aspects* **2002,** *207* (1), 89-104.
13. Ata, S.; Pugh, R. J.; Jameson, G. J., The influence of interfacial ageing and temperature on the coalescence of oil droplets in water. *Colloids Surf. Physicochem. Eng. Aspects* **2011,** *374* (1–3), 96-101.
14. Ayirala, S. C.; Al-Saleh, S. H.; Al-Yousef, A. A., Microscopic scale interactions of water ions at crude oil/water interface and their impact on oil mobilization in advanced water flooding. *Journal of Petroleum Science and Engineering* **2018,** *163*, 640-649.
15. Ayirala, S. C.; Yousef, A. A.; Li, Z.; Xu, Z., Coalescence of Crude Oil Droplets in Brine Systems: Effect of Individual Electrolytes. *Energy Fuels* **2018,** *32* (5), 5763-5771.
16. Won, J. Y.; Krägel, J.; Makievski, A. V.; Javadi, A.; Gochev, G.; Loglio, G.; Pandolfini, P.; Leser, M. E.; Gehin-Delval, C.; Miller, R., Drop and bubble micro manipulator (DBMM)—A unique

tool for mimicking processes in foams and emulsions. *Colloids Surf. Physicochem. Eng. Aspects* **2014,** *441*, 807-814.
17. Kamp, J.; Kraume, M., Influence of drop size and superimposed mass transfer on coalescence in liquid/liquid dispersions – Test cell design for single drop investigations. *Chem. Eng. Res. Des.* **2014,** *92* (4), 635-643.
18. Villwock, J.; Gebauer, F.; Kamp, J.; Bart, H.-J.; Kraume, M., Systematic Analysis of Single Droplet Coalescence. *Chemical Engineering & Technology* **2014,** *37* (7), 1103-1111.
19. Gebauer, F.; Villwock, J.; Kraume, M.; Bart, H.-J., Detailed analysis of single drop coalescence—Influence of ions on film drainage and coalescence time. *Chem. Eng. Res. Des.* **2016,** *115*, 282-291.
20. Luo, X.; Huang, X.; Yan, H.; Yang, D.; Zhang, P.; He, L., An experimental study on the coalescence behavior of oil droplet in ASP solution. *Sep. Purif. Technol.* **2018,** *203*, 152-158.
21. Bremond, N.; Bibette, J., Exploring emulsion science with microfluidics. *Soft Matter* **2012,** *8* (41), 10549-10559.
22. Krebs, T.; Schroen, K.; Boom, R., A microfluidic method to study demulsification kinetics. *Lab Chip* **2012,** *12* (6), 1060-1070.
23. Krebs, T.; Schroën, C. G. P. H.; Boom, R. M., Coalescence kinetics of oil-in-water emulsions studied with microfluidics. *Fuel* **2013,** *106*, 327-334.
24. Williams, Y. O. N.; Roas-Escalona, N.; Rodríguez-Lopez, G.; Villa-Torrealba, A.; Toro-Mendoza, J., Modeling droplet coalescence kinetics in microfluidic devices using population balances. *Chem. Eng. Sci.* **2019,** *201*, 475-483.
25. Zhou, Q.; Sun, Y.; Yi, S.; Wang, K.; Luo, G., Investigation of droplet coalescence in nanoparticle suspensions by a microfluidic collision experiment. *Soft Matter* **2016,** *12* (6), 1674-1682.
26. Liu, Z.; Cao, R.; Pang, Y.; Shen, F., The influence of channel intersection angle on droplets coalescence process. *Exp. Fluids* **2015,** *56* (2), 24.
27. Liu, Z.; Wang, X.; Cao, R.; Pang, Y., Droplet coalescence at microchannel intersection chambers with different shapes. *Soft Matter* **2016,** *12* (26), 5797-5807.
28. Wang, J.; Tan, S. H.; Nguyen, A. V.; Evans, G. M.; Nguyen, N.-T., A Microfluidic Method for Investigating Ion-Specific Bubble Coalescence in Salt Solutions. *Langmuir* **2016,** *32* (44), 11520-11524.
29. Nowbahar, A.; Whitaker, K. A.; Schmitt, A. K.; Kuo, T.-C., Mechanistic Study of Water Droplet Coalescence and Flocculation in Diluted Bitumen Emulsions with Additives Using Microfluidics. *Energy Fuels* **2017,** *31* (10), 10555-10565.
30. Lin, Y.-J.; Perrard, A.; Biswal, S. L.; Hill, R. M.; Trabelsi, S., Microfluidic Investigation of Asphaltenes-Stabilized Water-in-Oil Emulsions. *Energy Fuels* **2018**.
31. Wang, J.; Teo, A. J. T.; Tan, S. H.; Evans, G. M.; Nguyen, N.-T.; Nguyen, A. V., Influence of Interfacial Gas Enrichment on Controlled Coalescence of Oil Droplets in Water in Microfluidics. *Langmuir* **2019,** *35* (10), 3615-3623.
32. Yang, W.; Luo, Z.; Lai, Q.; Zou, Z., Study on bubble coalescence and bouncing behaviors upon off-center collision in quiescent water. *Exp. Therm Fluid Sci.* **2019,** *104*, 199-208.
33. Maeda, N.; Rosenberg, K. J.; Israelachvili, J. N.; Pashley, R. M., Further Studies on the Effect of Degassing on the Dispersion and Stability of Surfactant-Free Emulsions. *Langmuir* **2004,** *20* (8), 3129-3137.
34. Birdi, K. S., *Handbook of Surface and Colloid Chemistry*. CRC Press: Boca Raton, 2009.
35. Danov, K. D., Effect of Surfactants on Drop Stability and Thin Film Drainage. In *Fluid Mechanics of Surfactant and Polymer Solutions*, Starov, V.; Ivanov, I., Eds. Springer Vienna: Vienna, 2004; pp 1-38.
36. Hirasaki, G. J., Structural interactions in the wetting and spreading of van der Waals fluids. *J. Adhes. Sci. Technol.* **1993,** *7* (3), 285-322.
37. Yoon, Y.; Borrell, M.; Park, C. C.; Leal, L. G., Viscosity ratio effects on the coalescence of two equal-sized drops in a two-dimensional linear flow. *J. Fluid Mech.* **2005,** *525*, 355-379.

38. Dudek, M.; Muijlwijk, K.; Schroen, C. G. P. H.; Øye, G., The effect of dissolved gas on coalescence of oil drops studied with microfluidics. *J. Colloid Interface Sci.* **2018,** *528*, 166-173.
39. Cockbain, E. G.; McRoberts, T. S., The stability of elementary emulsion drops and emulsions. *Journal of Colloid Science* **1953,** *8* (4), 440-451.
40. Nielsen, L. E.; Wall, R.; Adams, G., Coalescence of liquid drops at oil-water interfaces. *Journal of Colloid Science* **1958,** *13* (5), 441-458.
41. Muijlwijk, K.; Li, X.; Berton-Carabin, C.; Schroën, K., Dynamic fluid interface formation in microfluidics: Effect of emulsifier structure and oil viscosity. *Innovative Food Science & Emerging Technologies* **2018,** *45*, 215-219.
42. He, Z.; Maldarelli, C.; Dagan, Z., The size of stagnant caps of bulk soluble surfactant on the interfaces of translating fluid droplets. *J. Colloid Interface Sci.* **1991,** *146* (2), 442-451.
43. Bao, B.; Riordon, J.; Mostowfi, F.; Sinton, D., Microfluidic and nanofluidic phase behaviour characterization for industrial CO2, oil and gas. *Lab Chip* **2017,** *17* (16), 2740-2759.
44. Vijayan, S.; Furrer, M.; Ponter, A. B., The effect of temperature on coalescence of liquid drops at liquid/liquid interfaces. *The Canadian Journal of Chemical Engineering* **1976,** *54* (4), 269-278.
45. Horn, R. G.; Del Castillo, L. A.; Ohnishi, S., Coalescence map for bubbles in surfactant-free aqueous electrolyte solutions. *Adv. Colloid Interface Sci.* **2011,** *168* (1), 85-92.
46. Del Castillo, L. A.; Ohnishi, S.; Horn, R. G., Inhibition of bubble coalescence: Effects of salt concentration and speed of approach. *J. Colloid Interface Sci.* **2011,** *356* (1), 316-324.
47. Pan, K. L.; Law, C. K., Dynamics of droplet–film collision. *J. Fluid Mech.* **2007,** *587*, 1-22.
48. Ozan, S. C.; Jakobsen, H. A., On the effect of the approach velocity on the coalescence of fluid particles. *Int. J. Multiphase Flow* **2019,** *119*, 223-236.
49. Liu, B.; Manica, R.; Liu, Q.; Klaseboer, E.; Xu, Z., Coalescence or Bounce? How Surfactant Adsorption in Milliseconds Affects Bubble Collision. *The Journal of Physical Chemistry Letters* **2019,** *10* (18), 5662-5666.